IJMMM International Journal of Minerals, Metallurgy and Materials 矿物冶金与材料学报（英文版）

An in-depth exploration of the performance and influence of rapid dewatering filter aid for red mud slurry

Le Tao, Yanxiu Wang, Wei Sun, Chengwen Wang, Li Wang, Zhiyong Gao, and Tingan Zhang

Cite this article as:
Le Tao, Yanxiu Wang, Wei Sun, Chengwen Wang, Li Wang, Zhiyong Gao, and Tingan Zhang, An in-depth exploration of the performance and influence of rapid dewatering filter aid for red mud slurry, *Int. J. Miner. Metall. Mater.*, 32(2025), No. 12, pp. 2896-2908. https://doi.org/10.1007/s12613-025-3096-8

View the article online at SpringerLink or IJMMM Webpage.

INTERNATIONAL JOURNAL OF
Minerals, Metallurgy and Materials

Volume 32, Number 12, December 2025
Page 2896

Research Article https://doi.org/10.1007/s12613-025-3096-8

An in-depth exploration of the performance and influence of rapid dewatering filter aid for red mud slurry

Le Tao[1,2], *Yanxiu Wang*[1,2)✉], *Wei Sun*[1,2)], *Chengwen Wang*[1,2)✉], *Li Wang*[1,2)], *Zhiyong Gao*[1,2)], *and Tingan Zhang*[3)]

1) School of Minerals Processing and Bioengineering, Central South University, Changsha 410083, China
2) Key Laboratory of Hunan Province for Clean and Efficient Utilization of Strategic Calcium-Containing Mineral Resources, Changsha 410083, China
3) School of Metallurgy, Northeastern University, Shenyang 110819, China
(Received: 8 November 2024; revised: 4 January 2025; accepted: 21 January 2025)

Abstract: Red mud is a kind of industrial waste residue produced in the process of alumina production, which has strong suspension and is difficult to precipitate and filter. This study compared the effects of 4 kinds of filter aids, including $CaCl_2$, polymerized ferrous sulfate (PFS), steel slag (SS), and Portland cement (PC), on the filtration rate, filter cake moisture content, and Na_2O content of red mud slurry. At a dosage of 10 g·L^{-1}, the filtration effects were in the following order: PFS > $CaCl_2$ > SS > PC. Under the combination of 5 g·L^{-1} SS and 5 g·L^{-1} PC, the better filtration effect was achieved with a filtration time of 205.17 s, which was reduced by 58.52% compared to the original red mud. The combined use of SS and PC exhibits better advantages in terms of cost and filtration effect. This study provides a data foundation for the rapid filtration of red mud slurry. The use of SS and PC as filter aids for red mud holds broad application prospects.

Keywords: red mud; filter aid; liquid–solid separation; interface regulation

1. Introduction

Red mud is an insoluble strong alkaline waste produced by fine grinding and strong alkali dissolution of bauxite at high temperature in the process of alumina production [1–3]. China is a major producer of alumina, and also the world's largest producer of red mud. In recent years, while alumina production has been increasing [4–5], the grade of bauxite has been decreasing. This has resulted in a growing amount of red mud produced for every ton of alumina, with accumulated stockpiles of red mud estimated to reach hundreds of millions of tons [6–7]. Common storage methods for red mud in China mainly include wet storage and dry storage. Due to its strong alkalinity, fine particle size and complex composition, red mud can cause very serious environmental harm if not treated properly. This may lead to pollution of ecosystems such as soil and groundwater [8–11], thereby presenting a significant challenge for the disposal of red mud.

In the Bayer process for alumina production, to minimize the adhesion loss of Al_2O_3 and Na_2O, red mud needs to undergo multiple washings, sedimentations, and filtrations to remove free alkali and achieve alkali solution circulation. This process aims to enhance the quality of alumina products and production efficiency. The sedimentation and filtration processes for red mud are intricate and time-consuming. To prevent secondary reaction losses of alumina, it is essential to rapidly accomplish the solid–liquid separation of red mud. However, the red mud contains a large number of fine particles after high-pressure leaching, with the particle size mainly distributed between 0.1 μm and 100 μm, resulting in poor settling performance [12–13]. Kumar and Kumar [14] determined the characteristic particle sizes (D_{10}, D_{50}, D_{90}) of red mud to be 0.37, 1.57, and 56.88 μm, indicating an extremely fine particle size distribution and a high content of fine particles. The abundance of fine particles makes it difficult to achieve effective separation through mechanical filtration, often leading to clogging of filtration equipment and slow filtration rates. Red mud is an alkaline slurry with a pH typically ranging from 10 to 12 [15]. At high pH levels, the particles in red mud generally carry a negative surface charge and exhibit strong electrostatic repulsion [16–17], which adversely affects settling and filtration processes [18]. These properties such as the fine particle size and strong alkalinity result in red mud having a high degree of suspension, making natural settling difficult and posing challenges for solid-liquid separation. The high specific surface area of red mud leads to strong adsorption [13], resulting in a higher moisture content in the filter cake after filtration. This also presents significant challenges for other production operations. Therefore, it is important to strengthen the liquid-solid separation

✉ Corresponding authors: Yanxiu Wang E-mail: 137141750@qq.com; Chengwen Wang E-mail: 215601026@csu.edu.cn

process of red mud slurry, promote the rapid dehydration of red mud, and realize the lye circulation.

Generally, liquid-solid separation and washing with a vacuum filter are required for the bottom stream of the final settlement of red mud. At present, the research on this filtration process mainly focuses on the development and improvement of special filters for red mud. Additionally, it is difficult to implement changes to large equipment in established industrial workshops, and equipment replacement is expensive. In contrast, the use of filter aids improves the filtration rate of the system and reduces the water content of the filter cake [19]. It is a simple and easy treatment with low investment and quick results, capable of automated operation. Filter aids are broadly classified into two basic types: medium-based aids (commonly referred to as filter aids in the chemical industry) and chemical filter aids. The latter category includes surfactant dewatering aids and flocculant filter aids [20]. By altering the physicochemical properties of particles in suspension [21–22], filter aids promote the aggregation, settling, and separation of suspended solids. This leads to improved pore distribution and connectivity within the filter cake. It facilitates the interception and separation of particles, thereby accelerating filtration speed and enhancing filtration performance. They can enhance filtration and dewatering performance with relatively low investment [23], without the need to alter existing processes. Common medium-based filter aids include materials like silica gel, activated carbon, diatomaceous earth, and cellulose, most of which are used in wastewater treatment. Medium-based filter aids mainly rely on the mechanical retention of particles to achieve filtration. Essakhraoui *et al*. [24] showed excellent filtration performance by using cellulose-based filter aid as a molten sulfur filter aid, which could reduce the amount of filter aid by one-third and effectively avoid the pollution of impurities.

Chemical filter aids have the capability to improve filtration efficiency and reduce filter cake moisture content. Flocculant filter aids can be categorized into natural and artificially synthesized, and are extensively applied in various fields including water treatment, mining, and metallurgy. Tan and Lu [25] found that using polyaluminum chloride as a filter aid to modulate the coal slurry interface could significantly improve the filtration rate and reduce the filtration time by 8.43 min compared with the blank test. Wang *et al*. [26] found that the new filter aid significantly improved the dewatering effect of coal preparation products by compressing the double electric layer and changing the surface hydrophobicity. Yan *et al*. [27] found that using poly(o-phenylenediamine)/poly dimethyl diallyl ammonium chloride (POPD/PDADMAC) composite filter aid significantly improved the dewatering effect of coal slime, and under the best experimental conditions, the filtration time was reduced from 83 to 53 s and the water content was decreased from 37.75wt% to 30.75wt%. Zhang *et al*. [28] found that sulfuric acid filter aid could compress the double electric layer on the surface of hematite concentrate particles to form larger particles, thus improving the filtration performance of fine hematite concentrate. Salamatov *et al.* [29] revealed that the use of polyacrylamide-based polymeric flocculants had a positive effect on the thickening process of red mud, but failed to promote the filtration of the red mud. Zeng *et al*. [15] studied the synergistic effect of surfactants, lime, and polyacrylamide (PAM) on the settling and dewatering of red mud. By neutralizing surface charges and adjusting surface wettability, the dewatering settling performance of red mud was improved, reducing the moisture content from 52.33wt% to 47.18wt%, and achieving a settling rate of 1.596 $m \cdot h^{-1}$. Patil and Thorat [30] investigated the effect of different filtration equipment on the filtration of red mud and found that hyperbaric steam pressure filtration can obtain a cake with >75wt% solids. Wang *et al*. [31] used the waste sand generated in slurry shield construction instead of lime as a filter aid to dehydrate the waste slurry generated in slurry shield tunneling construction more economically, which is a new environmentally friendly and economic way. In summary, chemical filter aids have been well studied for the treatment of fine particles that are difficult to filter, but few studies have been reported on the use of low-cost solid wastes to assist red mud filtration.

This study focuses on the filtration process of red mud. In the preliminary exploration experiment, 4 filter aids were selected from 12 filter aids including medium-based filter aids and chemical filter aids. In this paper, $CaCl_2$, polymerized ferrous sulfate (PFS), steel slag (SS), and Portland cement (PC) were studied and compared in detail. The reaction mechanism of the filter aid on the red mud filtration was analyzed by particle size determination, Zeta potential, optical microscopy and Fourier transform infrared spectroscopy (FTIR). Considering both the cost and environmental impact of the filter aids, a combination of preferred filter aids was identified to further enhance filtration efficiency and promote material recycling. An inorganic filter aid was developed using solid waste as a base material. It is low-cost, requires minimal usage, and achieves effective results, without impacting the composistion of red mud or subsequent production. This innovation significantly reduces costs and minimizes the impact on the aluminum oxide production process, leading to a substantial reduction in red mud filtration time, which is a novel and promising approach.

2. Experimental

2.1. Materials

The red mud used in this experiment was obtained from an alumina production enterprise in Shandong Province, China (C0). Additionally, the Bayer red mud samples from other plants are labeled as follows: C1 from Shandong Xinfa Aluminum Plant, China, C2 from an Aluminum Plant in Guizhou Province, China, C3 from an aluminum plant in Guangxi Province, China, and C4 from Guangxi Pingguo Aluminum Plant, China. The samples were finely ground to a particle size less than 74 μm and then dried in an oven. The main chemical components are shown in Table 1. $CaCl_2$ (purity $>$ 99%) used in the experiment was from Sinopharm Group Chemical Reagents Co., LTD., PFS (Fe content $\geq$ 21wt%) was from Shanghai Maclin Biochemical Technology Co., LTD., SS (300 mesh) came from a steel smelter in

Hubei Province, China, and PC (300 mesh) came from Henan Tianrui Group, China. The chemical compositions of SS and PC are shown in Table 1. The SS contains relatively higher mass fractions of CaO and Fe_2O_3. In contrast, the PC has a CaO content as high as 64.43wt%, while its Fe_2O_3 content is relatively low.

As shown in Fig. 1(a), raw red mud primarily contains phases such as Hematite (Fe_2O_3), Gibbsite ($Al(OH)_3$), Boehmite (γ-AlOOH), Carnegieite ($NaAlSiO_4$), Anatase (TiO_2), Natrolite ($Na_2Al_2Si_3O_{10}\cdot 2H_2O$) and Quartz ($SiO_2$). Based on the Mineral Liberation Analyzer (MLA), a backscattered electron image (BSE) (Fig. 1(b)) and corresponding energy spectrum image (Fig. 1(c)) were obtained to comprehensively analyze the phase distribution of red mud. Non-clay minerals such as iron oxides in red mud are enveloped and aggregated under the influence of clay minerals. The presence of clay minerals and impurities leads to a sharp increase in the content of fine particles. The viscosity of red mud slurry increases, posing challenges to the difficulty of liquid-solid separation.

2.2. Experimental process

At the beginning of the experiment, 16.67 g of red mud and 50 mL of water were added to a 200 mL beaker according to the liquid-solid ratio of 3:1. Then it was placed in a constant temperature digital water bath to stir and heat for 30 min while maintaining a temperature of 60°C and a stirring speed of 300 $r\cdot min^{-1}$ to obtain red mud slurry. The initial pH was around 12.

During the experiment, a blank experiment was carried out without filter aid as a control group. It has been determined that the filtration time for the control group was 494.67 s, with moisture content of 40.06wt% and Na_2O content of 6.88wt%. Then, 4 kinds of filter aids were added to the pulp at the dosage of 1, 5, and 10 $g\cdot L^{-1}$, respectively, for parallel testing. The mixture was then stirred for 3 min. After stirring, the red mud slurry was promptly poured into the funnel for filtration. The circulating water multi-purpose vacuum pump was used to maintain constant pressure filtration. The filtrate was put into a 100 mL measuring cylinder in the filter bottle to record the filtration time. The time required for every 5 mL of filtrate to pass through was recorded until the filtration was completed. After that, the wet weight of the filter cake was recorded and the dry weight was recorded by drying. Finally, the sample was tested for Na_2O content. The main experimental process is depicted in Fig. 2. The specific experimental conditions are designed in Table 2.

2.3. Characterization methods

Experimental equipment includes a circulating water multi-purpose vacuum pump, constant-temperature digital display water bath, oven, 80-mm Buchner funnel, 1000-mL suction filtration bottle, 100-mL measuring cylinder, beaker, and electronic balance. The experimental water used is tap

Table 1. The main chemical compositions of experimental material wt%

Material	Composition						
	Al_2O_3	SiO_2	CaO	Fe_2O_3	Na_2O	TiO_2	Others
C0	20.53	13.11	1.36	40.07	16.24	6.76	1.93
C1	21.30	15.92	1.97	32.88	19.03	7.39	1.51
C2	19.71	16.70	14.14	29.43	11.45	4.46	4.11
C3	18.61	12.27	17.29	28.45	11.93	8.20	3.25
C4	25.28	6.28	3.65	51.65	4.91	6.08	2.15
SS	Al_2O_3	SiO_2	CaO	Fe_2O_3	MnO	MgO	Others
	2.04	13.33	44.13	26.36	4.57	5.21	4.36
PC	Al_2O_3	SiO_2	CaO	Fe_2O_3	SO_3	MgO	Others
	4.86	16.31	64.43	2.98	4.75	3.73	2.94

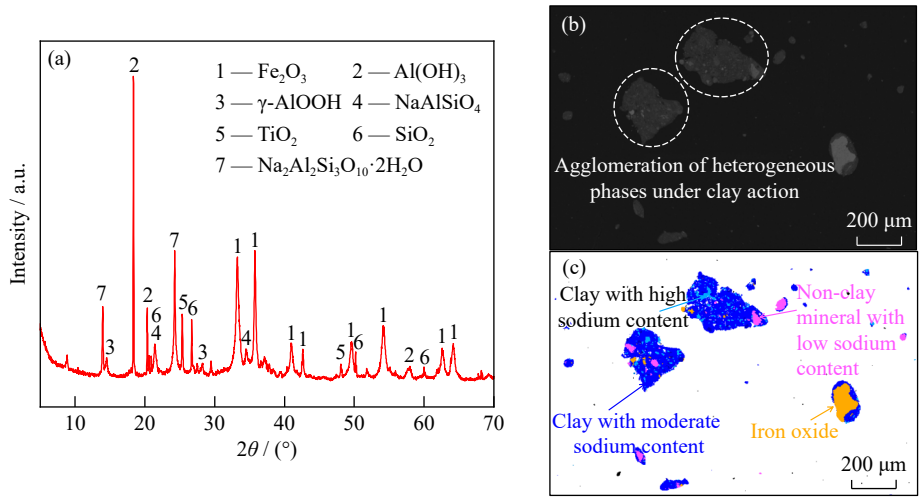

Fig. 1. (a) X-ray powder diffraction pattern of red mud; (b) BSE image; (c) phase distribution map.

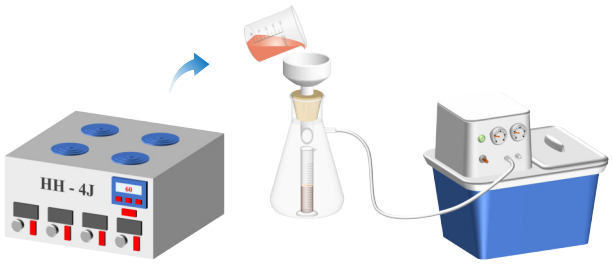

Fig. 2. Main process diagram of the filtration experiment.

water. The chemical composition of the red mud was analyzed using an X-ray fluorescence spectrometer (Axios mAX, PANalytical, Netherlands). The red mud sample was subjected to phase analysis using an X-ray diffractometer (XRD) with a scanning range from −3° to 162°, Cu K_α radiation (PANalytical, Germany). The model of the instrument used to detect the particle size distribution of the experimental sample is Mastersizer 2000 with Hydro2000M (Malvern, UK), and the scan speed for sample measurement is 1000 s^{-1}. The Zeta potential analyzer used in the experiment was the model Malvern Zetasizer Nano ZS (Mal ZEN3600/nano ZS, UK). The effect of filter aids on the agglomeration behavior of red mud slurry was observed with a DM RXP polarized light microscope (Leica, Germany). FTIR (Thermo Fisher Scientific Nicolet iS20, USA) was used to characterize the structural changes of SS and PC before and after hydrolysis under alkaline conditions. The elemental content of SS and PC dissolved under alkaline conditions was detected by inductively coupled plasma optical emission spectrometer (ICP-OES, Spectro Blue SOP).

2.4. Technological concept

Fig. 3 illustrates the diagram of the technological concept. Through the preliminary basic research, macroscopic experiment and effect analysis have been completed. Subsequently, the combination and optimization are carried out. Following this approach, 4 potential filter aids were initially screened including $CaCl_2$, PFS, SS, and PC. To identify low-cost and highly effective filter aids for red mud dewatering, comparative experiments were conducted on the types and quantities of these filter aids. The impact of different categories of filter aids on red mud filtration performance was evaluated based on indicators such as red mud filtration time, filter cake alkalinity, and moisture content. Combination experiments with different ratios of the selected filter aids were conducted to investigate the synergistic effects of different types and quantities of filter aids on red mud filtration. The reaction mechanism of the filter aid to promote agglomeration of red

Table 2. The experimental design matching parameter table

No.	Red mud	Weight of red mud / wt%	Type of filter aid	Dosage of filter aid / ($g \cdot L^{-1}$)	T / °C	Liquid–solid ratio
1	C0	16.67	—	—	60	3:1
2	C0	16.67	$CaCl_2$	1	60	3:1
3	C0	16.67	$CaCl_2$	5	60	3:1
4	C0	16.67	$CaCl_2$	10	60	3:1
5	C0	16.67	PFS	1	60	3:1
6	C0	16.67	PFS	5	60	3:1
7	C0	16.67	PFS	10	60	3:1
8	C0	16.67	SS	1	60	3:1
9	C0	16.67	SS	5	60	3:1
10	C0	16.67	SS	10	60	3:1
11	C0	16.67	PC	1	60	3:1
12	C0	16.67	PC	5	60	3:1
13	C0	16.67	PC	10	60	3:1
14	C0	16.67	SS + $CaCl_2$	9 + 1	60	3:1
15	C0	16.67	PC + $CaCl_2$	9 + 1	60	3:1
16	C0	16.67	SS + PC	5 + 5	50	3:1
17	C0	20.00	SS + PC	5 + 5	60	2.5:1
18	C0	16.67	SS + PC	5 + 5	60	3:1
19	C0	12.50	SS + PC	5 + 5	60	4:1
20	C0	16.67	SS + PC	5 + 5	70	3:1
21	C1	16.67	SS + PC	5 + 5	60	3:1
22	C1	16.67	SS + PC	5 + 5	60	3:1
23	C2	16.67	SS + PC	5 + 5	60	3:1
24	C2	16.67	SS + PC	5 + 5	60	3:1
25	C3	16.67	SS + PC	5 + 5	60	3:1
26	C3	16.67	SS + PC	5 + 5	60	3:1
27	C4	16.67	SS + PC	5 + 5	60	3:1
28	C4	16.67	SS + PC	5 + 5	60	3:1

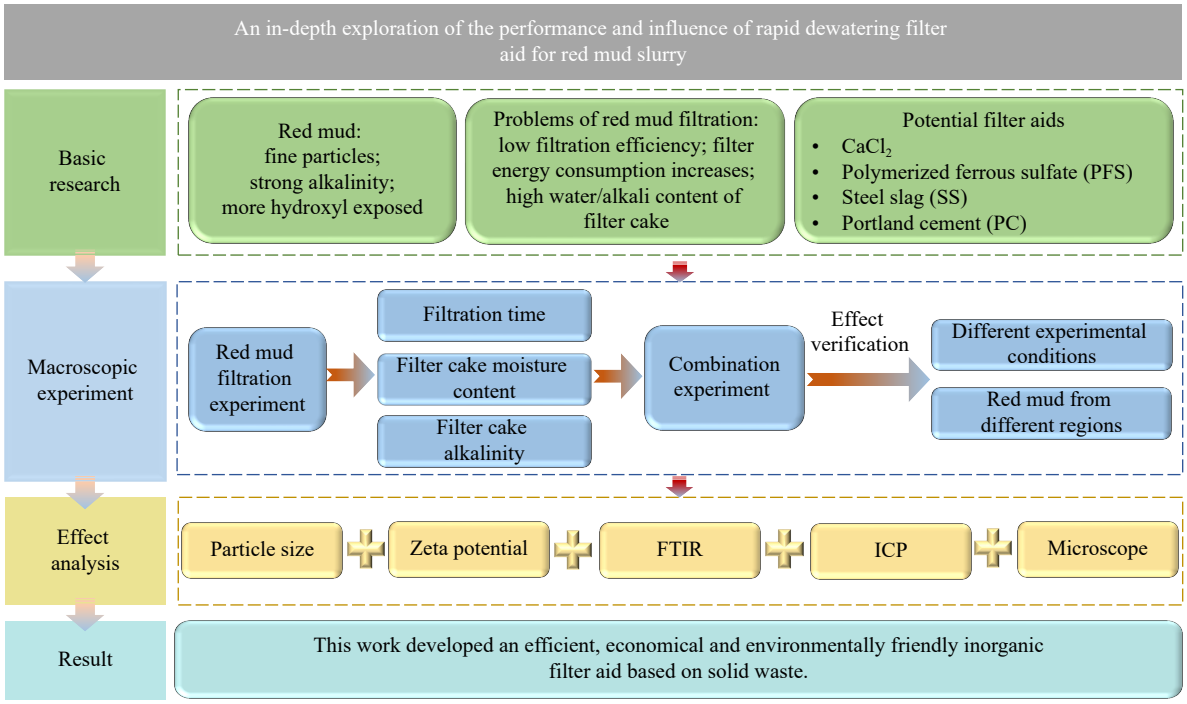

Fig. 3. Diagram of the technological concept.

mud slurry was analyzed by particle size determination, Zeta potential, optical microscopy and FTIR. In order to verify the performance of filter aid under different working conditions, validation tests were carried out under different temperature and liquid-solid ratios. In order to verify the universality of filter aid, experiments were carried out on red mud from different sources. The study concluded with the development of an efficient and fast dewatering filter aid for red mud slurries. This opens up a new avenue for the development of red mud filter aids based on solid waste materials.

3. Results and discussion

3.1. Impact of various filter aids on the filtration efficiency of red mud

Fig. 4(a) indicates that the use of $CaCl_2$ can effectively shorten the filtration time. The filtration effect at a dosage of 10 g·L^{-1} is significantly better than at 1 and 5 g·L^{-1}. The filtration time was 269.98 s (1 g·L^{-1}), 294.49 s (5 g·L^{-1}), and 192.63 s (10 g·L^{-1}), which is 54.58%, 59.53%, and 38.94% of the filtration time without filter aid (494.67 s). The moisture content of the filter cake was 37.53wt%, 37.48wt%, and 38.87wt%, respectively, which is 2.53wt%, 2.58wt%, and 1.19wt% lower than that of the blank group (Fig. 4(b)). Due to the strong hydration ability of Ca^{2+}, the surface hydration film of red mud particles is relatively thick, resulting in a higher moisture content in the filter cake. The Na_2O content was 6.37wt%, 6.19wt%, and 6.14wt%, respectively, showing obvious reduction. Particles in red mud typically carry a negative charge, resulting in a repulsive effect between them. This makes it difficult for red mud to aggregate and settle [32]. Ca^{2+} can react with colloidal particles or suspended solids in solution, altering their surface charge and thereby forming larger flocs [33–34]. These flocs increase the size and density of the particles, promoting their aggregation and settling. This improves the filtration efficiency. The interaction between Ca^{2+} and red mud particles neutralizes the surface charge, reducing the repulsive force between particles (Fig. 4(c)). It is conducive to the aggregation and settling of red mud particles, thereby enhancing the filter aid effect. Fig. 4(d) indicates that the filter aid effect of PFS followed the order of 10 g·L^{-1} (189.43 s) > 5 g·L^{-1} (226.42 s) > 1 g·L^{-1} (341.15 s). The filtration time is accordingly 38.29%, 45.77%, and 68.97% of the time taken without the addition of a filter aid, respectively. The filter aid effect is quite significant at dosages of 5 and 10 g·L^{-1}. However, the cake moisture content increased with the dosage, measuring 35.50wt%, 37.88wt%, and 40.52wt% respectively. The Na_2O content was reduced noticeably, measuring 6.52wt%, 6.31wt%, and 6.10wt% (Fig. 4(e)). PFS ($[Fe_2(OH)_n(SO_4)_{3-n/2}]_m$ ($n < 2$, $m > 10$)) [35] is a commonly used cationic inorganic polymer filter aid employed in water treatment processes for the removal of suspended solids and turbidity. The filter aid capability of PFS arised from its functions in charge neutralization, compression of the double electric layer, and reduction of colloid Zeta potential [36]. PFS solution contains many polymeric iron complexes. These complexes can reduce the negative charge on the surface of red mud particles, decrease the mutual repulsion between particles, and cause the particles to bind together and facilitate particle aggregation and settling (Fig. 4(f)). Additionally, its porous structure and coagulation bridging action can improve the cake structure and promote the filtration process.

Fig. 4(g) indicates that at three different dosages, the filtering rate of red mud slurry with SS is relatively fast. The filtration time decreased from 494.67 to 253.39, 244.77, and 236.16 s, which is 51.22%, 49.48%, and 47.74% of the blank group. The moisture content of the filter cake was 37.11wt%,

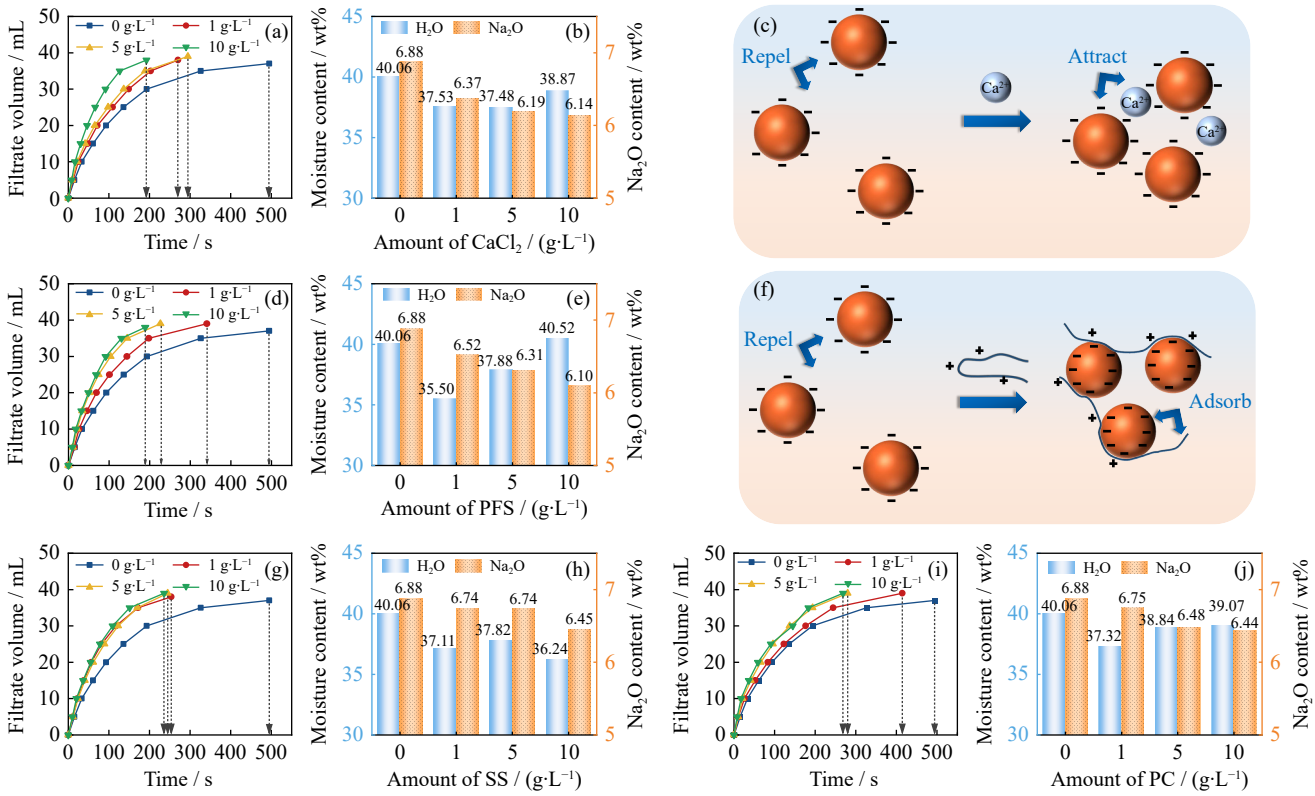

Fig. 4. Filtration time under different dosages of (a) $CaCl_2$, (d) PFS, (g) SS, and (i) PC (liquid–solid ratio is 3:1, temperature is 60°C); filter cake moisture content and Na_2O content of (b) $CaCl_2$, (e) PFS, (h) SS, and (j) PC; (c) mechanism schematic diagram of $CaCl_2$; (f) mechanism schematic diagram of PFS.

37.82wt%, and 36.24wt%, which is 2.95wt%, 2.24wt%, and 3.82wt% lower compared to the blank group (Fig. 4(h)). The main components of SS are oxides of calcium, iron, magnesium, and silicon. Previous experiments [15] have demonstrated that CaO can effectively neutralize the surface anions of red mud particles, compress the double electric layer, reduce the hydration film, and improve filtration efficiency. Additionally, the surface of SS exhibits certain adsorption activity, which can enhance the liquid-solid separation efficiency by adsorbing certain substances in the solution through physical and chemical adsorption [37]. As a cheap industrial waste, the reuse of SS as a filter aid to improve the filtration efficiency of red mud reflects the concept of "using waste to treat waste". The use of SS can also reduce some costs. Moreover, it reduces the impact on subsequent processes due to its composition being similar to red mud, showing promising application prospects. As shown in Fig. 4(i), the addition of PC reduced the filtration time from 494.67 s to 414.27, 280.07, and 268.79 s, which is 83.75%, 56.62%, and 54.34% of the blank group. The reduction in filtration time is significant at PC dosages of 5 and 10 $g \cdot L^{-1}$. The moisture contents of the filter cake at the three dosages were 37.32wt%, 38.84wt%, and 39.07wt%, respectively, which were 2.74wt%, 1.22wt%, and 0.99wt% lower than the blank group (Fig. 4(j)). Due to the increased filtration rate, the corresponding filter cake moisture content is also higher. PC is primarily composed of CaO, SiO_2, Fe_2O_3, and Al_2O_3 [38], which is similar in composition to SS.

$CaCl_2$ and PFS exhibit the best filtration effects with filtration time of 192.63 and 189.43 s at a dosage of 10 $g \cdot L^{-1}$. Compared to the blank experiment group, the filtration time was reduced by 61.06% and 61.71%. However, they are relatively expensive leading to higher production costs. SS and PC follow with filtration time of 236.16 and 268.79 s at a dosage of 10 $g \cdot L^{-1}$. These two filter aid systems were able to reduce the filtration time of red mud by 52.26% and 45.66%.

3.2. Filter aids compounding experiment

In order to further improve the filtration efficiency of red mud, the preferred filter aid is combined and configured to promote the synergy between minerals. The results in Fig. 5 show the filtration time for different filter aids: $CaCl_2$ (10 $g \cdot L^{-1}$), SS (10 $g \cdot L^{-1}$), PC (10 $g \cdot L^{-1}$), SS (5 $g \cdot L^{-1}$) + PC (5 $g \cdot L^{-1}$), SS (9 $g \cdot L^{-1}$) + $CaCl_2$ (1 $g \cdot L^{-1}$), and PC (9 $g \cdot L^{-1}$) + $CaCl_2$ (1 $g \cdot L^{-1}$). When compounding 9 $g \cdot L^{-1}$ of SS with 1 $g \cdot L^{-1}$ of $CaCl_2$, the filtration time is 248.12 s, and the filtration time is shortened by 49.84%. Similarly, when compounding 9 $g \cdot L^{-1}$ of PC with 1 $g \cdot L^{-1}$ of $CaCl_2$, the filtration time was 245.65 s, and the filtration time was shortened by 50.34%. Surprisingly, when compounding 5 $g \cdot L^{-1}$ of SS with 5 $g \cdot L^{-1}$ of PC, the filtration time was 205.17 s, which is 58.52% shorter than the filtration time of the raw red mud slurry. This is superior to using SS or PC alone as filter aids, and the compounding effect is close to the best effect achieved with $CaCl_2$. Both SS and PC are relatively inexpensive, yet their combination can achieve filtration results comparable to using $CaCl_2$ alone as a filter aid. SS as an industrial solid waste comes at a low cost, while PC is a widely

used cementing material. This significantly reduces production costs. Moreover, the chemical composition of SS and PC closely resembles that of red mud, ensuring no impact on the composition of sodium aluminate solution and minimizing effects on the quality and production cycle of aluminum oxide products.

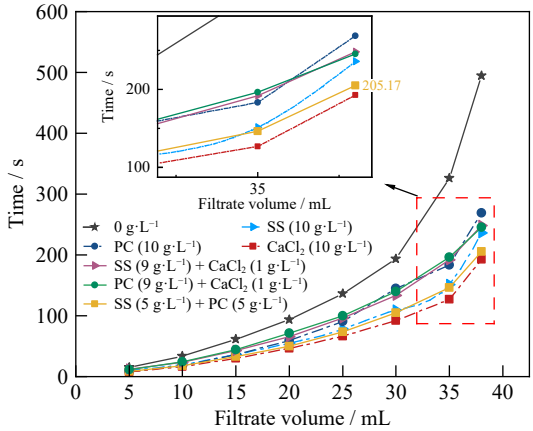

Fig. 5. Compound filter aids filtration time diagram (liquid–solid ratio is 3:1, temperature is 60°C).

3.3. Influence of different single factor conditions on filtration effect of red mud

To investigate the working conditions in actual industrial production, the effects of single-factor conditions, such as temperature and liquid–solid ratio, on the filtration performance of red mud slurry after multiple countercurrent washings were investigated. Under the condition of SS + PC combination (dosage of 5 $g \cdot L^{-1}$ + 5 $g \cdot L^{-1}$), filtration experiments were conducted on C0, with the results presented in Fig. 6.

Under the condition of the liquid–solid ratio of 3:1 (Fig. 6(a)), the filtration time decreases with increasing temperature, though the reduction is relatively small. Specifically, the filtration time is 234.16 s at 50°C, 205.17 s at 60°C, and 186.79 s at 70°C. This trend indicates that higher temperatures reduce liquid viscosity and enhance liquid flow, thereby facilitating the filtration process [39]. Additionally, as temperature increases, the compressibility of the sample decreases [40], resulting in reduced compactness of the filter cake, which further benefits the dewatering process.

At the fixed red mud slurry temperature of 60°C (Fig. 6(b)), filtration becomes difficult at lower liquid-solid ratios due to the higher viscosity and strong suspension properties of the slurry. When the liquid–solid ratio reaches 4, the number of particles decreases, allowing the particles to disperse more easily in the liquid, significantly improving filtration and dewatering efficiency. However, the higher liquid–solid ratio leads to a significant increase in the moisture content of the filter cake, making it a burden for subsequent processing. In summary, the effect of temperature on red mud filtration time is minor, with a 20°C increase in temperature reducing filtration time by 20.23%. In contrast, increasing the liquid–solid ratio from 2.5 to 4 reduces filtration time by 29.98%. However, maintaining higher temperatures entails increased energy consumption, and a higher liquid–solid ratio leads to greater water usage. Therefore, it is necessary to comprehensively consider the addition of filter aids and the single-factor conditions for filtration based on actual site conditions and the observed trends. This approach maximizes filtration efficiency and minimizes the cost of red mud filtration. In this experiment, the temperature of 60°C and the liquid–solid ratio of 3 were selected as the best experimental conditions.

3.4. Applicability verification of different red mud filtration

In order to further verify the universality of SS + PC as the filter aid, red mud from 4 different regions was selected to comprehensively evaluate the filtration effect. Filtration experiments were conducted using SS + PC combination (5 $g \cdot L^{-1}$ + 5 $g \cdot L^{-1}$) as described in Section 2.2, with results presented in Fig.7. Under the influence of SS + PC, the filtration time for all red mud samples significantly decreased. Specifically, the filtration time for C1 reduced from 284.51 to 166.47 s, C2 from 109.49 to 71.14 s, C3 from 121.89 to 96.91 s, and C4 from 526.70 to 245.76 s. Notably, C1 and C4 exhibited relatively longer initial filtration times, indicating greater filtration difficulty, while SS + PC markedly improved their filtration efficiency. In contrast, C2 and C3 had shorter initial filtration times, suggesting easier filtration, and thus the improvement by SS + PC was less pronounced. This

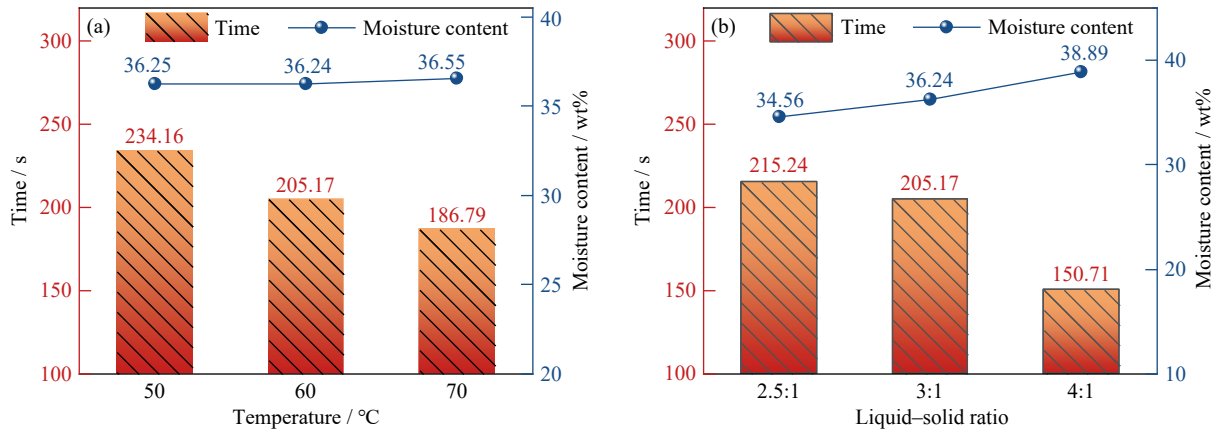

Fig. 6. (a) Filtration time of C0 at different temperatures; (b) filtration time of C0 under different liquid–solid ratios.

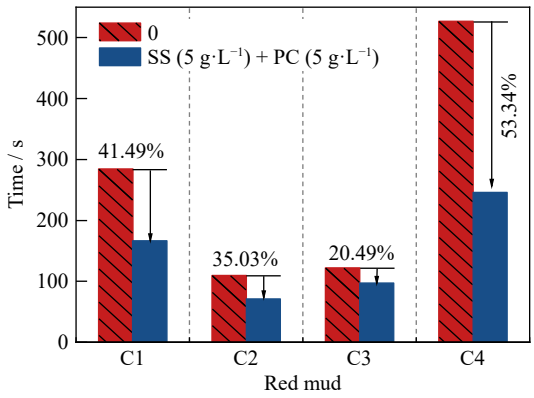

Fig. 7. Filtration time of red mud in different regions (liquid–solid ratio is 3:1, temperature is 60°C).

variation in filtration behavior can be attributed to differences in the chemical composition of the red mud samples. Specifically, higher CaO content enhances filtration efficiency through the action of Ca^{2+}. The experimental findings demonstrate that SS + PC exhibits good universality across different red mud systems, suggesting its broader applicability in various red mud systems.

3.5. Agglomeration behavior and reaction mechanism

3.5.1. Variation of particle size

The effects of $CaCl_2$, PFS, SS, PC, and SS + PC on the red mud particle size were measured at 3wt% (relative red mud solid phase content), respectively. Fig. 8 shows the analysis results of particle size changes. Table 3 provides correspond-

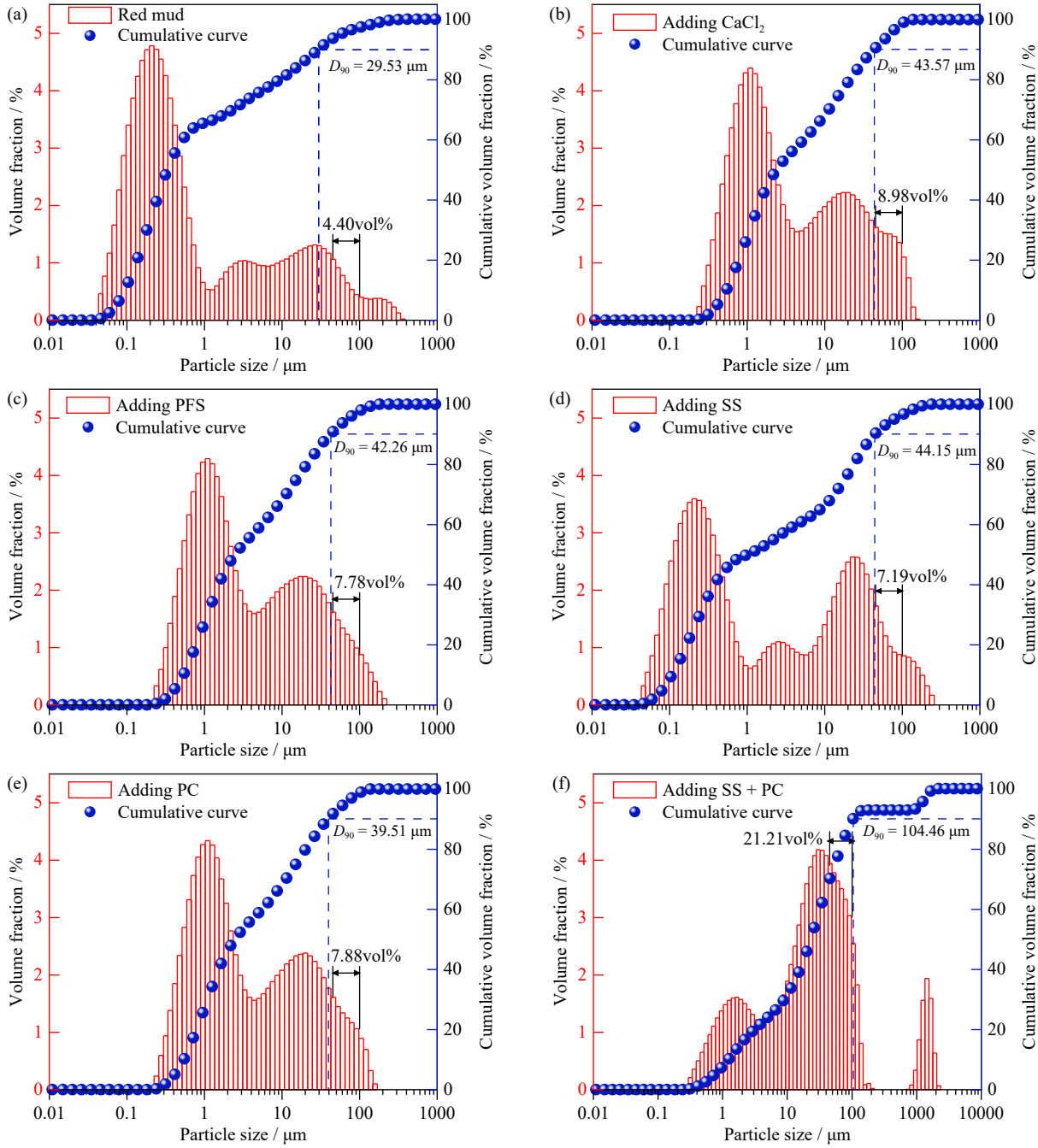

Fig. 8. Volume fraction and cumulative content curve for each particle size of red mud: (a) red mud; (b) after adding $CaCl_2$; (c) after adding PFS; (d) after adding SS; (e) after adding PC; (f) after adding SS+PC.

Table 3. The specific surface area, surface area average particle size (D_s), and volume average particle size (D_v) of red mud and red mud after adding filter aid

Category	Specific surface area / ($m^2 \cdot g^{-1}$)	D_s / μm	D_v / μm
Red mud	25.80	0.233	10.922
Red mud after adding $CaCl_2$	4.25	1.412	13.583
Red mud after adding PFS	4.25	1.411	14.252
Red mud after adding SS	19.40	0.309	15.576
Red mud after adding PC	4.21	1.424	13.086
Red mud after adding SS + PC	1.49	4.032	122.329

ing data results for specific surface area, surface area average particle size, and volume average particle size.

The particle size distribution of red mud is fine, with 90% of the particles being smaller than 29.526 μm. The content of particles in the range of 0.1–1 μm is 65.44wt%, while that in the range of 1–100 μm is 31.62wt%. The addition of filter aids results in an increase in the average particle size of red mud particles, a decrease in the number of particles in the range of 0.1–1 μm, and an increase in the number of particles in the range of 1–100 μm. The volume average particle size (D_v) increases from 10.922 to 15.576 μm (adding SS), 13.086 μm (adding PC), 13.583 μm (adding $CaCl_2$), and 14.252 μm (adding PFS). Fedorova *et al*. [41] found that when a certain amount of flocculant was added to treat red mud, the content of particles in the range of 45–100 μm reached 70wt%, indicating that the distribution of slurry particle size can reflect the flocculation effect from the side. In this experiment, as shown in Fig. 8, the content of red mud particles in the range of 45–100 μm after treatment with filter aids was 8.98vol%($CaCl_2$), 7.78vol% (PFS), 7.19vol% (SS), and 7.88vol% (PC), respectively, which was significantly higher than the 4.40wt% of the raw red mud. Obviously, the volume average particle size of the slurry increases to 122.329 μm when SS and PC are used in combination. Furthermore, the specific surface area of the particles decreases from 25.80 to 1.49 $m^2 \cdot g^{-1}$. Compared with other filter aids, the combined configuration of SS and PC significantly increases the particle content in the range of 45–100 μm, and there are mineral aggregates at the 1000 μm scale. The increase in the volume average particle sizes of red mud particles and the reduction in the number of fine particles indicate that the addition of inorganic filter aids promotes the aggregation of fine particles. The formation of larger particles accelerates the liquid-solid separation process, improves the filter cake structure, and consequently reduces filtration time. That is, the reduction of fine particles and the increase of volume average particle size can improve the filtration rate [42].

3.5.2. Microscopic morphology

Fig. 9 shows the optical microscope images at different magnifications after addition of SS (10 $g \cdot L^{-1}$), PC (10 $g \cdot L^{-1}$) and SS + PC combination (5 $g \cdot L^{-1}$ + 5 $g \cdot L^{-1}$). As shown in Fig. 9(a), the raw red mud has a uniform particle distribution with a high number of fine particles. Part of the small particles are aggregated to form large loosely structured particles, and the overall state is stable. After the addition of SS (Fig. 9(b)), it can be observed that significant agglomeration occurred between the red mud particles. Small particles bond to each other to form aggregates. Some of the aggregates are in contact with each other to form lumpy loose bodies. It can be clearly observed that the gaps between the block aggregates are significantly increased. After the addition of PC (Fig.9(c)), the red mud particles formed flocculent aggregates, and the number of fine particles decreased. This result is similar to the particle size variation of red mud in the SS system. Under the synergistic effect of the composite filter aids (Fig. 9(d)), the agglomeration behavior of the red mud was further enhanced, and the network-like agglomeration structure was gradually formed. At a scale of 25 μm, it can be observed that the agglomerates are clustered together by medium agglomerates of different particle sizes and morphologies. Meanwhile, loose mineral particles can be further found adhering around large agglomerates or between pores. This suggests that the minerals are in contact with each other by some kind of action behavior.

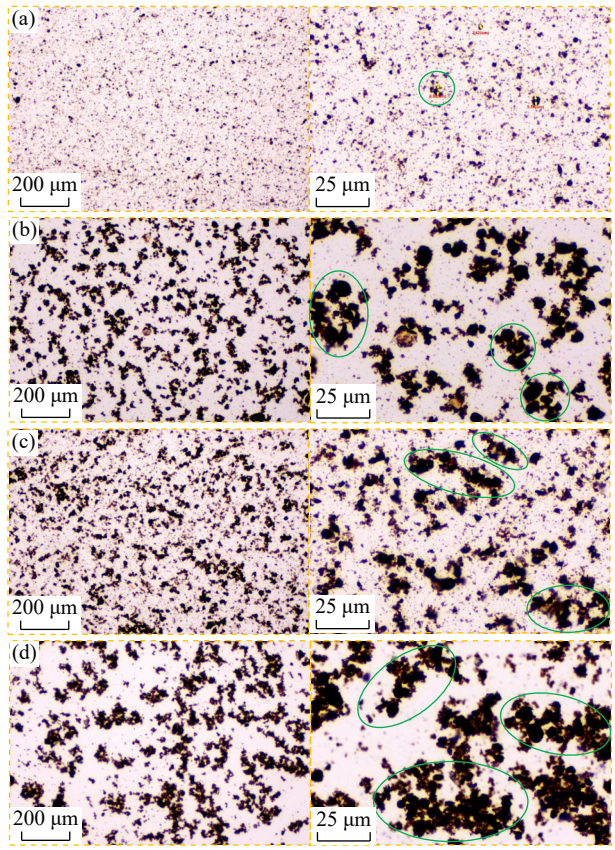

Fig. 9. Microscopic morphology: (a) original red mud slurry; (b) red mud slurry after adding SS; (c) red mud slurry after adding PC; (d) red mud slurry after adding SS + PC.

3.5.3. Reaction behavior and agglomeration mechanism

Fig. 10(a) presents the results of the Zeta potential testing. The Zeta potential of red mud without any added filtration aid is about −41 mV. In different kinds of filter aid systems, the overall trend of Zeta potential changes on the surface of red mud particles was similar. The addition of $CaCl_2$ and PFS resulted in a more pronounced decrease in the absolute value of the Zeta potential on the surface of red mud. With the gradual increase in dosage, the surface of red mud is positively charged. This indicates that their ability to neutralize the negative charge is significantly stronger than that of SS and PC. However, in the combined configuration of SS and PC, the red mud surface potential increased from about −41 to −10 mV. This suggests that SS and PC can also have the effect of neutralizing the negative charge of the red mud surface.

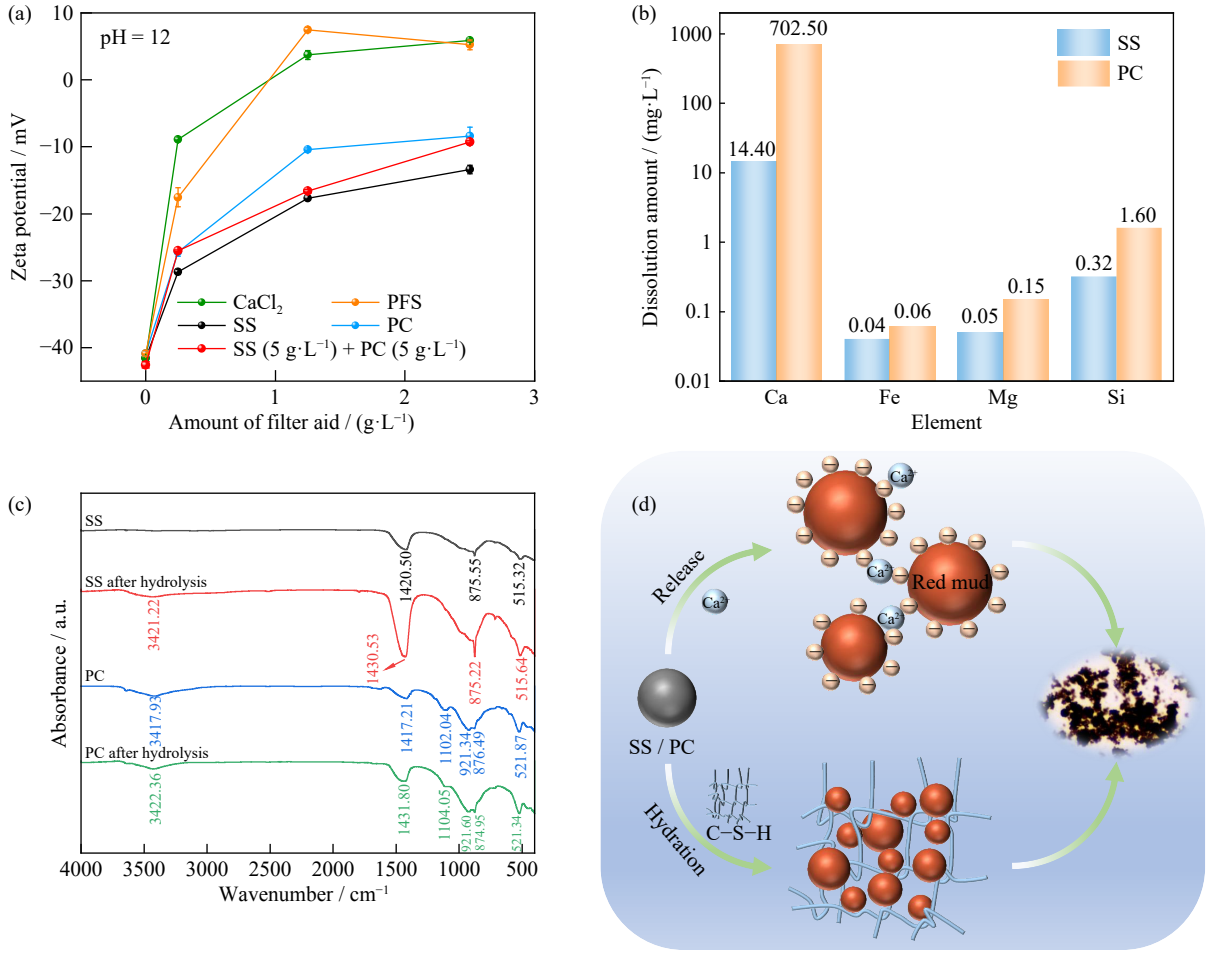

Fig. 10. (a) Zeta potential diagram; (b) elemental distribution of SS and PC after hydrolysis in alkali solution; (c) Fourier-transform infrared spectra of SS and PC after hydrolysis in alkali solution; (d) mechanism diagram of agglomeration.

Fig. 10(b) shows the elemental distribution of SS and PC after dissolution in an alkaline environment. The polyvalent metal ions dissolved in the two filter aid systems are mainly Ca^{2+}, Mg^{2+}, and Fe^{3+}/Fe^{2+}. Among them, the dissolution of Ca^{2+} is predominant, with the dissolution amount being about 14.4 mg·L^{-1} for SS and 702.5 mg·L^{-1} for PC. The dissolved Ca^{2+} neutralizes the surface potential of the red mud and reduces the charge density, which leads to a decrease in electrostatic repulsion. Therefore, it is easier for small particles to be converted into large aggregates by electrostatic attraction [43]. This result is consistent with the experimental phenomena in sections 3.5.1 and 3.5.2.

Fig.10(c) shows the FTIR spectra of SS and PC before and after hydrolysis in an alkaline environment. The 1420.50 cm^{-1} and 875.55 cm^{-1} in the raw SS are CO_3^{2-} antisymmetric stretching vibration and out-of-plane bending vibration in $CaCO_3$ [44]. The characteristic peak at 515.32 cm^{-1} is the bending vibration of the Si–O–Si bond in calcium silicate gel (C–S–H) [45]. After the hydrolysis of the SS, the absorption bands of CO_3^{2-} at 1430.53 and 875.22 cm^{-1} were enhanced, indicating that the free calcium oxide dissolved in the alkaline environment to form $Ca(OH)_2$ [46], which then reacted with CO_2 in the air to form $CaCO_3$. A new O–H bond stretching vibration at 3421.22 cm^{-1} suggests that some degree of hydration has occurred in the SS [47]. Additionally, the intensity of the characteristic peak of the Si–O–Si bond at 515.64 cm^{-1} increased, suggesting that the hydrolysis process increased the C–S–H generation. The 1417.21 and 874.95 cm^{-1} in the raw PC are the CO_3^{2-} antisymmetric stretching vibration in $CaCO_3$. 912.04 and 1102.04 cm^{-1} are the asymmetric and symmetric stretching vibration of the Si–O bond; 521.87 cm^{-1} is the vibration peak of the Si–O

bond in hydrated calcium silicate gel (C–S–H) [48]. After hydrolysis of PC, the antisymmetric stretching vibration of CO_3^{2-} in $CaCO_3$ appeared and strengthened in the higher band of 1431.80 cm^{-1}. The vibration peak intensity of the Si–O bond at 921.60 and 521.34 cm^{-1} increased. This indicates that PC and SS are similar in an alkaline environment, accompanied by the dissolution of Ca^{2+} and the formation of C–S–H. The C–S–H gel has a large specific surface area, strong surface activity, and a dense three-dimensional mesh structure [49], which is capable of wrapping the dispersed red mud to form large particles. As shown in Fig. 10(d), SS and PC reduced the surface charge of red mud and formed a C–S–H cross-linked network. The agglomeration of red mud was promoted by the synergistic effect of the two behaviors.

3.6. Economic assessment

The combination and utilization of the respective characteristics of SS and PC synergistically improve the filtration speed and stability to achieve the best filtration effect. The advantages of using solid waste as a filter aid can be further demonstrated by cost estimates in combination with industrial red mud filtration configurations. Under optimal process conditions, filtering 1 ton of red mud was used as the unit of cost estimation, as shown in Table 4. $CaCl_2$ and PFS are able to reduce the filtration time by 61%–62%, but the treatment cost for 1 ton of red mud is about 3 $ or more. The combination of SS and PC reduces the filtration time by 58.52% and the treatment cost for 1 ton of red mud is about 0.5–1 $. Therefore, under the condition of similar filtration time, the combination of SS and PC can highlight the larger advantages in terms of operating costs. Therefore, this work research provides a reference for the industrial treatment of microfine-grained red mud.

Table 4. Cost comparison of filter aids for filtering 1 ton of red mud

Filter aids	Price / ($·$t^{-1})	Dosage / t	Cost / $
$CaCl_2$	285–300	0.030	8.55–9.00
PFS	100–255	0.030	3.00–7.65
SS	5–10	0.030	0.15–0.30
PC	28–60	0.030	0.84–1.80
SS + PC	—	0.015 + 0.015	0.50–1.05

Note: Refer to Alibaba Mall for raw material prices (alibaba.com).

4. Conclusions

The research investigated filter aids impact on filtration time, addressing the issues of high cost associated with existing organic coagulants used in the red mud solid–liquid separation process, which negatively affects the quality of alumina products. This study fills the gap for low-cost, efficient, and fast-dehydrating inorganic filter aids for red mud slurry. The following conclusions are based on these studies.

(1) Four inorganic filter aids were identified that significantly improved the filtration rate of red mud: $CaCl_2$, PFS, SS, and PC. Compared to the filtration time without any added filter aids, these filter aids reduced the filtration time by 61.06%, 61.71%, 52.26%, and 45.66%, respectively.

(2) Using SS (5 g·L^{-1}) + PC (5 g·L^{-1}) as the filter aid for red mud filtration yielded excellent overall results. Compared to direct red mud filtration, the filtration time was reduced by 58.52%, indicating a significant improvement in filtration efficiency.

(3) SS and PC can reduce the surface charge of red mud particles, in addition, the formation of C–S–H and the cross-linking between the particles, promote the agglomeration of red mud particles and accelerate the filtration speed.

(4) The use of SS + PC as the filter aid embodies the concept of "using waste to treat waste", achieving the recycling of resources and reducing environmental pollution. At the same time, it has great advantages in operating costs.

Currently, the application of filter aids is relatively limited, showing effectiveness primarily in red mud filtration, with minimal use in other difficult-to-filter slurries. Future research will explore the application of these filter aids in other difficult-to-filter systems to expand their scope and promote resource reuse. At the same time, attention should be given to potential adverse effects that may arise in different difficult-to-filter systems.

Acknowledgements

This work was supported by the Science and Technology Innovation Program of Hunan Province, China (No. 2023RC3053), the National Key Research and Development Program of China (No. 2023YFC3904201), and the National Natural Science Foundation of China (No. 52004343).

Conflict of Interest

The authors declare that there is no conflict of interest.

References

[1] E. Mukiza, L.L. Zhang, and X.M. Liu, Durability and microstructure analysis of the road base material prepared from red mud and flue gas desulfurization fly ash, *Int. J. Miner. Metall. Mater.*, 27(2020), No. 4, p. 555.

[2] B.C. Trampus and S.C.A. França, Performances of two flocculants and their mixtures for red mud dewatering and disposal based on mineral paste production, *J. Cleaner Prod.*, 257(2020), art. No. 120534.

[3] T.Y. Cai, M. Yang, and R.X. Pan, Study on the effect of sodium removal from citric acid pretreated red mud on the physical properties of red mud, *Environ. Sci. Pollut. Res.*, 31(2024), No. 31, p. 44191.

[4] Y.T. Xu, B. Yang, X.M. Liu, *et al.*, Investigation of the medium calcium based non-burnt brick made by red mud and fly ash: Durability and hydration characteristics, *Int. J. Miner. Metall. Mater.*, 26(2019), No. 8, p. 983.

[5] G.T. Zhou, Y.L. Wang, T.G. Qi, *et al.*, Comparison of the effects of Ti- and Si-containing minerals on goethite transformation in the Bayer digestion of goethitic bauxite, *Int. J. Miner.*

Metall. Mater., 30(2023), No. 9, p. 1705.
[6] G. Power, M. Gräfe, and C. Klauber, Bauxite residue issues: I. Current management, disposal and storage practices, *Hydrometallurgy*, 108(2011), No. 1-2, p. 33.
[7] Y.F. Huang, G.H. Han, J.T. Liu, and W.J. Wang, A facile disposal of Bayer red mud based on selective flocculation desliming with organic humics, *J. Hazard. Mater.*, 301(2016), p. 46.
[8] M. Johnston, M.W. Clark, P. McMahon, and N. Ward, Alkalinity conversion of bauxite refinery residues by neutralization, *J. Hazard. Mater.*, 182(2010), No. 1-3, p. 710.
[9] S.B. Rai, K.L. Wasewar, R.S. Mishra, *et al*., Sequestration of carbon dioxide in red mud, *Desalin. Water Treat.*, 51(2013), No. 10-12, p. 2185.
[10] S. Agrawal, V. Rayapudi, and N. Dhawan, Microwave reduction of red mud for recovery of iron values, *J. Sustain. Metall.*, 4(2018), No. 4, p. 427.
[11] Y.B. Zong, W.H. Chen, Y. Fan, T.L. Yang, Z.B. Liu, and D.Q. Cang, Complementation in the composition of steel slag and red mud for preparation of novel ceramics, *Int. J. Miner. Metall. Mater.*, 25(2018), No. 9, p. 1010.
[12] F. Jones, J.B. Farrow, and W. van Bronswijk, Flocculation of haematite in synthetic bayer liquors, *Colloids Surf. A*, 135(1998), No. 1-3, p. 183.
[13] J.Z. Zhang, Z.Y. Yao, K. Wang, *et al*., Sustainable utilization of bauxite residue (Red Mud) as a road material in pavements: A critical review, *Constr. Build. Mater.*, 270(2021), art. No. 121419.
[14] A. Kumar and S. Kumar, Development of paving blocks from synergistic use of red mud and fly ash using geopolymerization, *Constr. Build. Mater.*, 38(2013), p. 865.
[15] H. Zeng, H.H. Tang, W. Sun, and L. Wang, Deep dewatering of bauxite residue *via* the synergy of surfactant, coagulant, and flocculant: Effect of surfactants on dewatering and settling properties, *Sep. Purif. Technol.*, 302(2022), art. No. 122110.
[16] D. Chvedov, S. Ostap, and T. Le, Surface properties of red mud particles from potentiometric titration, *Colloids Surf. A*, 182(2001), No. 1-3, p. 131.
[17] K.Y. Zhang, H.P. Hu, L.J. Zhang, and Q.Y. Chen, Surface charge properties of red mud particles generated from Chinese diaspore bauxite, *Trans. Nonferrous Met. Soc. China*, 18(2008), No. 5, p. 1285.
[18] G.J. Liang, A.V. Nguyen, W.M. Chen, T.A.H. Nguyen, and S. Biggs, Interaction forces between goethite and polymeric flocculants and their effect on the flocculation of fine goethite particles, *Chem. Eng. J.*, 334(2018), p. 1034.
[19] A.S. Yang, Y.F. Liao, M.Y. An, *et al*., Effect of surfactant and flocculant on low-rank coal slime filtration: From filter cake characteristics point of view, *Fuel*, 327(2022), art. No. 125136.
[20] X.M. Hu, *Chemical Filter Aids*, Metallurgical Industry Press, Beijing, 1999, p. 46.
[21] X.F. You, M. He, X.C. Zhu, *et al*., Influence of surfactant for improving dewatering of brown coal: A comparative experimental and MD simulation study, *Sep. Purif. Technol.*, 210(2019), p. 473.
[22] R.X. Chen, X.S. Dong, Y.P. Fan, X.M. Ma, Y.D. Dong, and M. Chang, Interaction between STAC and coal/kaolinite in tailing dewatering: An experimental and molecular-simulation study, *Fuel*, 279(2020), art. No. 118224.
[23] W.Z. Yin, Y. Xie, and Z.L. Zhu, Literature overview of basic characteristics and flotation laws of flocs, *Int. J. Miner. Metall. Mater.*, 31(2024), No. 5, p. 943.
[24] M. Essakhraoui, A. Nyassi, A. Boukhair, *et al*., Enhancing molten sulfur filtration during sulfuric acid manufacturing for phosphate fertilizer production in Morocco with cellulose-based filter aids, *Appl. Sci.*, 13(2023), No. 15, art. No. 8879.
[25] X.F. Tan and J. Lu, Study on the application of inorganic salt filter aid in slime filtration, *China Coal*, 49(2023), No. 2, p. 109.
[26] T.Y. Wang, J. Chen, H.H. Shang, L.X. Bao, G.Q. Yu, and J. Tian, Hydrophobic regulation enhances the filtration and dehydration for coal preparation products, an experimental exploration, *Physicochem. Probl. Miner. Process.*, 60(2024), No. 6, art. No. 194659.
[27] X.H. Yan, L.B. Wei, and H.X. Xu, Synergistic enhancement of dewatering of montmorillonite-containing coal slime by novel combined filter aid: An experimental and simulation study, *Int. J. Coal Prep. Util.*, (2024), p. 1.
[28] J.L. Zhang, Y.F. Guo, F.Q. Zheng, S. Wang, F. Chen, and L.Z. Yang, High efficiency filtration and optimization of pelletizing performance of fine hematite concentrate using sulfuric acid filter aid: Behavior and mechanism, *Powder Technol.*, 448(2024), art. No. 120260.
[29] V.I. Salamatov, O.V. Salamatov, and D. Yu Zabolotnyaya, K-4 impact on dehydration process of red mud settling, [in] *Proceedings of the IOP Conference Series:Earth and Environmental Science*, 988(2022), art. No. 022030.
[30] S.V. Patil and B.N. Thorat, Mechanical dewatering of red mud, *Sep. Purif. Technol.*, 294(2022), art. No. 121157.
[31] D.F. Wang, F.L. Min, H.J. Lyu, J. Chen, B.T. Wang, and J.F. Zhang, Recycling waste sand from slurry shield tunneling: A sustainable filter aid for waste slurry dehydration, *J. Cleaner Prod.*, 383(2023), art. No. 135387.
[32] H. Zeng, H.H. Tang, W. Sun, and L. Wang, Strengthening solid–liquid separation of bauxite residue through the synergy of charge neutralization and flocculation, *Sep. Purif. Technol.*, 285(2022), art. No. 120296.
[33] J. Long, H. Li, Z. Xu, and J.H. Masliyah, Role of colloidal interactions in oil sand tailings treatment, *AlChE J.*, 52(2006), No. 1, p. 371.
[34] J. Walsch and S. Dultz, Effects of pH, Ca- and SO_4-concentration on surface charge and colloidal stability of goethite and hematite–consequences for the adsorption of anionic organic substances, *Clay Miner.*, 45(2010), No. 1, p. 1.
[35] W.P. Cheng, Hydrolysis characteristic of polyferric sulfate coagulant and its optimal condition of preparation, *Colloids Surf. A*, 182(2001), No. 1-3, p. 57.
[36] Z. Li, C.H. Li, Y.Q. Meng, *et al*., Application of coagulation and full-membrane process in municipal reclaimed water in northern China: An optimized process, *Desalin. Water Treat.*, 217(2021), p. 159.
[37] C.H. Shi, X.C. Wang, S. Zhou, X.M. Zuo, and C. Wang, Mechanism, application, influencing factors and environmental benefit assessment of steel slag in removing pollutants from water: A review, *J. Water Process. Eng.*, 47(2022), art. No. 102666.
[38] P.E. Stutzman, Microscopy of clinker and hydraulic cements, *Rev. Mineral. Geochem.*, 74(2012), No. 1, p. 101.
[39] Z.X. Xu, Z.M. Li, S.T. Cui, *et al*., Assessing the performance of foams stabilized by anionic/nonionic surfactant mixture under high temperature and pressure conditions, *Colloids Surf. A*, 651(2022), art. No. 129699.
[40] J. Hulston, R.G. de Kretser, and P.J. Scales, Effect of temperature on the dewaterability of hematite suspensions, *Int. J. Miner. Process.*, 73(2004), No. 2-4, p. 269.
[41] E. Fedorova, E. Pupysheva, and V. Morgunov, Modelling of red-mud particle-solid distribution in the feeder cup of a thickener using the combined CFD-DPM approach, *Symmetry*, 14(2022), No. 11, art. No. 2314.
[42] R. Salimi and J. Vaughan, Crystallisation of tricalcium aluminate from sodium aluminate solution using slaked lime, *Powder Technol.*, 294(2016), p. 472.
[43] F.Q. Zheng, Y.F. Guo, J.J. Fan, *et al*., R31 filter aid enhances filtration of fine hematite concentrate particles, *Powder Technol.*, 378(2021), p. 255.
[44] T.W. Zheng, X. Zhang, and H.H. Yi, Spherical vaterite micro-

spheres of calcium carbonate synthesized with poly (acrylic acid) and sodium dodecyl benzene sulfonate, *J. Cryst. Growth*, 528(2019), art. No. 125275.

[45] M.S. Li, H. Liu, P. Duan, S.Q. Ruan, Z.H. Zhang, and W. Ge, The effects of lithium slag on microstructure and mechanical performance of metakaolin-based geopolymers designed by response surface method (RSM), *Constr. Build. Mater.*, 299(2021), art. No. 123950.

[46] B. Bai, F. Bai, Q.K. Nie, and X.X. Jia, A high-strength red mud–fly ash geopolymer and the implications of curing temperature, *Powder Technol.*, 416(2023), art. No. 118242.

[47] N. Çöpoğlu, H. Gökdemir, T. Cengiz, and B. Çiçek, Barium borosilicate glass coatings based on biomass for steel surfaces: Use of rice husk ash, *Ceram. Int.*, 48(2022), No. 6, p. 8671.

[48] P. Yu, R. James Kirkpatrick, B. Poe, P.F. McMillan, and X.D. Cong, Structure of calcium silicate hydrate (C–S–H): Near-, mid-, and far-infrared spectroscopy, *J. Am. Ceram. Soc.*, 82(1999), No. 3, p. 742.

[49] S.J. Chen, Z.W. Du, Z. Zhang, D.W. Yin, F. Feng, and J.B. Ma, Effects of red mud additions on gangue-cemented paste backfill properties, *Powder Technol.*, 367(2020), p. 833.